

Atomic structure of alloy surfaces. III. $\text{Ni}_3\text{Al}\{110\}$

D. Sondericker* and F. Jona

College of Engineering and Applied Science, State University of New York at Stony Brook, Stony Brook, New York 11794-2275

P. M. Marcus

IBM Thomas J. Watson Research Center, P.O. Box 218, Yorktown Heights, New York 10598

(Received 30 June 1986)

A low-energy-electron-diffraction intensity analysis of a clean and annealed $\{110\}$ surface of Ni_3Al reveals that the first layer is 50% Ni–50% Al and that the second layer is 100% Ni. In the first layer, the Ni and Al subplanes are slightly separated from one another by 0.02 ± 0.03 Å, the Al atoms being outwards from the bulk. The first interlayer distance, as measured from the Ni subplane, is contracted by 0.15 ± 0.03 Å (11.9% of the bulk value, 1.26 Å). The second interlayer distance is expanded by 0.04 ± 0.03 Å (3% of the bulk value). The r -factor values for normal (0.14) and oblique (0.13) incidence indicate a very good fit of theory to experiment.

I. INTRODUCTION

In two articles we have reported on the atomic structure of $\{001\}$ [paper I (Ref. 1)] and $\{111\}$ [preceding article, paper II (Ref. 2)] surfaces of Ni_3Al as determined by analysis of low-energy electron diffraction (LEED) intensities. The mean relaxations found on these surfaces are similar to those found on $\{001\}$ and $\{111\}$ surfaces of face-centered-cubic metals² (typically 2% or 3% contraction to 1% expansion of the first interlayer spacing), but the most noteworthy new feature of the alloy surfaces is buckling, i.e., different relaxations of the different alloy partners. On $\text{Ni}_3\text{Al}\{001\}$ the Ni and Al subplanes in the first atomic layer separate by only 0.02 ± 0.03 Å, and on $\text{Ni}_3\text{Al}\{111\}$ by 0.06 ± 0.03 Å, but on $\text{NiAl}\{110\}$ they separate by 0.22 Å (see Davis and Noonan³). We show that in $\text{Ni}_3\text{Al}\{110\}$ the mean relaxation also corresponds to the observed values for the $\{110\}$ surface of pure metals, but the buckling is surprisingly small in view of the $\text{NiAl}\{110\}$ result. Trends, both in the mean relaxation and in the buckling, cannot yet be recognized because the available experimental data are scarce (see references in paper II). The present paper increases the data base for identifying such trends by reporting on the structure of another surface of Ni_3Al , the $\{110\}$ surface.

Figure 1 shows a schematic view of the bulk unit cell of Ni_3Al (an ordered alloy with the Cu_3Au structure) with a $\{110\}$ plane highlighted. It is apparent that there are two possible $\{110\}$ terminations, one with a unit mesh containing one Al and one Ni atom in the first layer and two Ni atoms in the second layer (mixed-layer termination, bottom left in Fig. 1), the other with the reverse order, i.e., a unit mesh containing two Ni atoms in the first, and one Al and one Ni in the second layer (Ni-layer termination, bottom right in Fig. 1). This question of terminations is similar to that encountered in the $\langle 001 \rangle$ direction, where two terminations are also possible, although both size and symmetry of the unit mesh on $\{001\}$ and $\{110\}$ are of course different. The LEED analysis reported in paper I shows that on $\{001\}$ surfaces the stable termination is the mixed-layer plane. The LEED analysis described below

shows that on $\{110\}$ surfaces the same conclusion holds true. We present in Sec. II some experimental details, in Sec. III the analysis, and in Sec. IV the conclusions.

II. EXPERIMENT

The source of the $\{110\}$ sample used in this study was the same ingot that provided the $\{001\}$ and the $\{111\}$ sample. Surface preparation and cleaning were similar to those done for $\{001\}$. Argon-ion bombardments of 1 hr/cycle were followed by 950°C anneals of 1 hr/cycle; before collection of LEED intensity data anneals were done at 700°C and followed by slow cooling. Ten cycles were done before collection of the data used in the analysis.

Chemical composition and relative stability of the surface were monitored with Auger-electron spectroscopy (AES), particularly after argon-ion bombardments. Figure 2 shows the ratio $R_A = I(\text{Al}_{68\text{eV}})/I(\text{Ni}_{61\text{eV}})$ between the intensities of the (doubly differentiated) AES lines of Al at 68 eV and Ni at 61 eV (for a precise definition of R_A see paper I, footnote 2) as a function of annealing temperature (10-min annealing time at each temperature). As is also found on the $\{001\}$ and $\{111\}$ surfaces, immediately after ion bombardment the surface is always Ni rich, indicating that Al is preferentially sputtered. Upon heating, Al diffuses onto the surface until a relatively stable composition is reached (plateau in Fig. 2). Further heating reactivates the Al enrichment of the surface but slow cooling to room temperature reestablishes approximately the stable composition. The intensity data used in the LEED analysis were collected from a surface with this stable composition. Since the results of this analysis, to be presented below, indicate that the top layer has 50% Al–50% Ni composition, it is surprising to find that R_A is smaller on the $\{110\}$ surface (~ 0.71) than on the $\{001\}$ surface (~ 0.95). A possible explanation for this fact is that since the interlayer spacing along $\langle 110 \rangle$ is smaller (by about 30%) than that along $\langle 001 \rangle$ more layers are probed by AES and hence R_A is closer to the

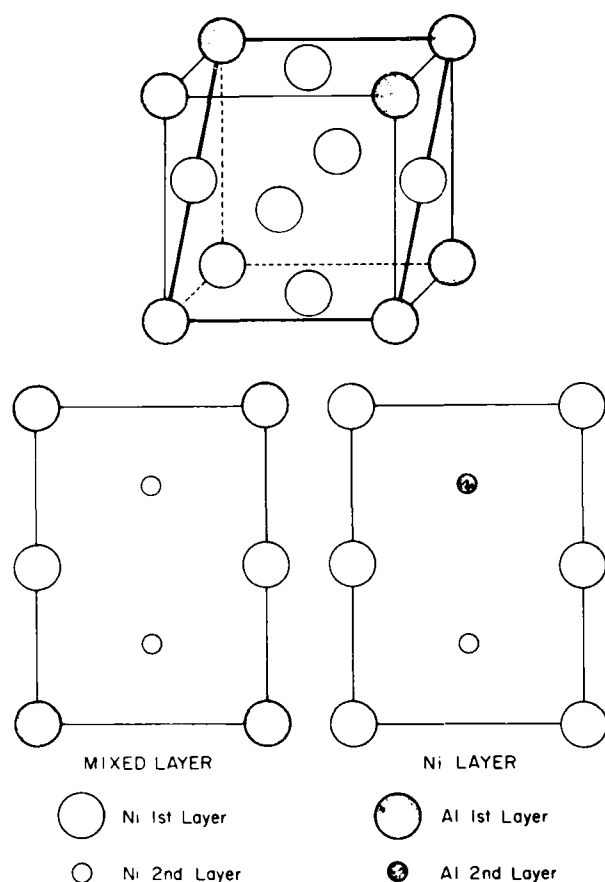


FIG. 1. Schematic unit cell of the Ni_3Al structure with $\{110\}$ plane emphasized. Top views of possible $\{110\}$ terminations are shown on bottom left (mixed layer) and bottom right (Ni layer).

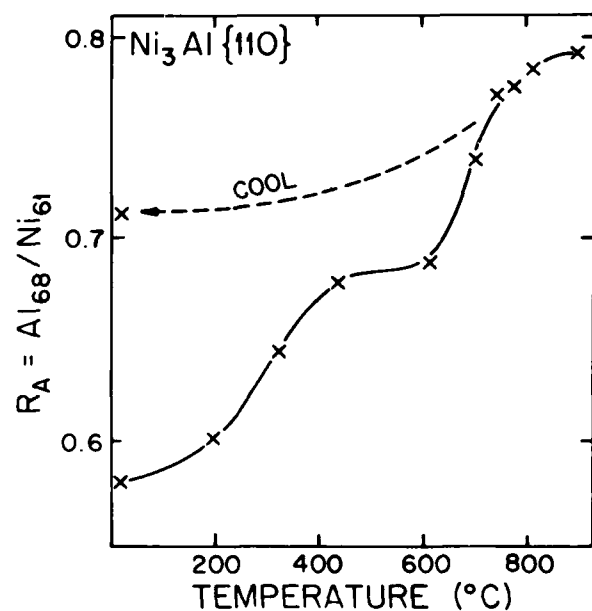


FIG. 2. Effect of (10-min) anneals at the temperature given on the abscissa axis upon the ratio R_A of intensities of AES lines of Al at 68 eV and Ni at 61 eV.

TABLE I. Beam indices, r (reliability) factors, and energy ranges for $\text{Ni}_3\text{Al}\{110\}$ at normal incidence. $V_0 = 12$ eV.

| Beam | r factor | ΔE |
|------------------|------------|------------|
| 10 | 0.1918 | 168 |
| $\bar{1}0$ | 0.1976 | 167 |
| 01 | 0.1338 | 154 |
| $0\bar{1}$ | 0.1568 | 159 |
| 11 | 0.1233 | 164 |
| $\bar{1}\bar{1}$ | 0.1199 | 159 |
| 20 | 0.2128 | 111 |
| $\bar{2}0$ | 0.1567 | 111 |
| 02 | 0.1295 | 156 |
| $0\bar{2}$ | 0.1292 | 154 |
| 22 | 0.1300 | 94 |
| $\bar{2}\bar{2}$ | 0.1326 | 94 |
| 12 | 0.0472 | 145 |
| $\bar{1}\bar{2}$ | 0.0561 | 145 |
| $\bar{1}\bar{2}$ | 0.0594 | 146 |
| $1\bar{2}$ | 0.0641 | 145 |
| 21 | 0.1047 | 89 |
| $2\bar{1}$ | 0.1030 | 89 |
| 03 | 0.2256 | 94 |
| $0\bar{3}$ | 0.2542 | 94 |
| $\bar{1}\bar{3}$ | 0.0955 | 55 |
| 13 | 0.2091 | 89 |
| $\bar{1}\bar{3}$ | 0.2282 | 89 |
| $1\bar{3}$ | 0.2004 | 89 |
| Mean 0.1409 | | 2958 |

TABLE II. Beam indices, r (reliability) factors, and energy ranges for $\text{Ni}_3\text{Al}\{110\}$ at $\theta = 15^\circ$, $\phi = 90^\circ$. $V_0 = 13$ eV.

| Beam | r factor | ΔE |
|------------------|------------|------------|
| 00 | 0.2617 | 172 |
| 10 | 0.0598 | 160 |
| $\bar{1}0$ | 0.0832 | 167 |
| 01 | 0.4092 | 105 |
| $0\bar{1}$ | 0.1037 | 165 |
| $\bar{1}\bar{1}$ | 0.0802 | 155 |
| $1\bar{1}$ | 0.1008 | 162 |
| 20 | 0.1319 | 53 |
| $\bar{2}0$ | 0.1976 | 54 |
| $0\bar{2}$ | 0.0871 | 92 |
| $2\bar{2}$ | 0.1078 | 94 |
| $\bar{2}\bar{2}$ | 0.1140 | 105 |
| $1\bar{2}$ | 0.1156 | 155 |
| $\bar{1}\bar{2}$ | 0.0862 | 135 |
| $2\bar{1}$ | 0.1936 | 115 |
| $2\bar{1}$ | 0.1241 | 95 |
| $1\bar{3}$ | 0.0625 | 135 |
| $2\bar{3}$ | 0.0435 | 70 |
| Mean 0.1280 | | 2189 |

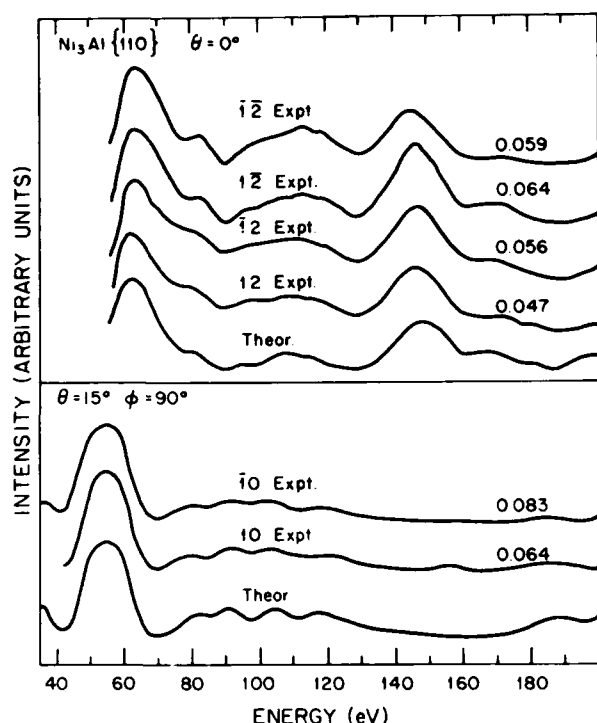


FIG. 3. Examples of very good fit of theory to experiment. The numbers above the experimental curves are r -factor values.

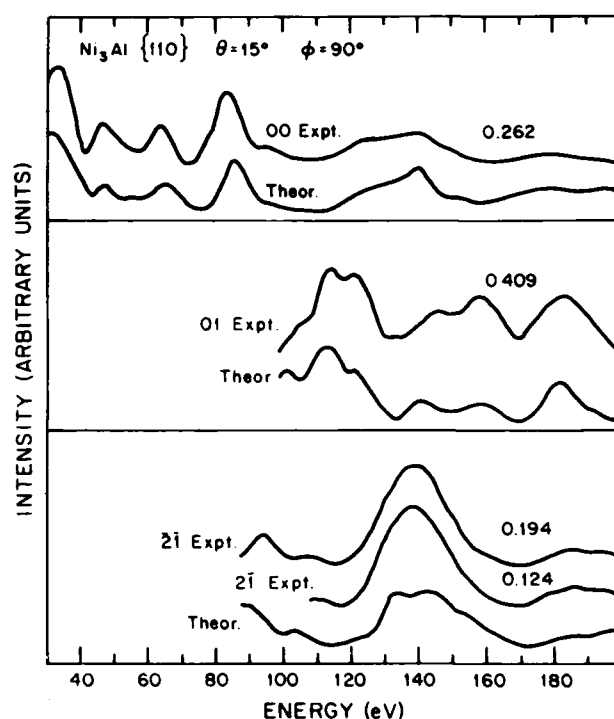


FIG. 5. Examples of poor fit of theory to experiment. The numbers above the experimental curves are r -factor values.

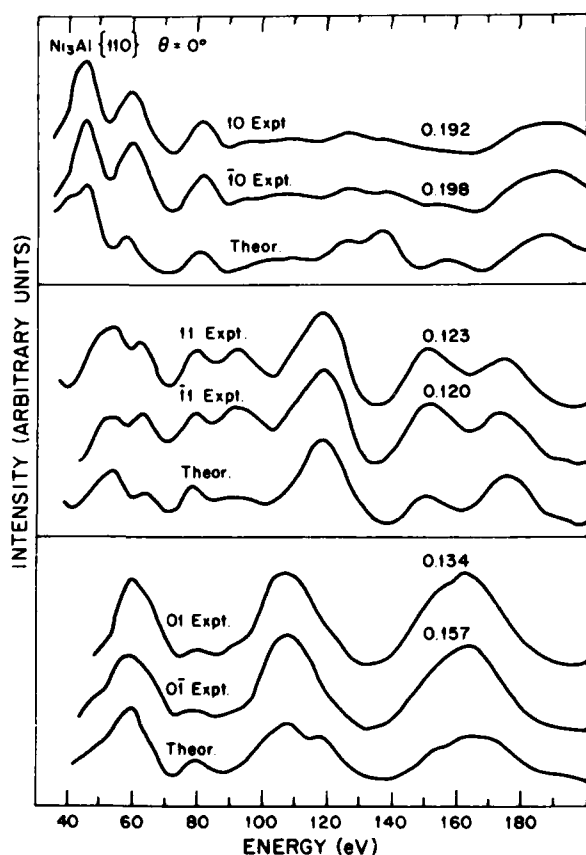


FIG. 4. Examples of good to mediocre fit of theory to experiment. The numbers above the experimental curves are r -factor values.

bulk value in the former than in the latter case (for the {111} termination, which has the bulk composition in all layers, R_A is 0.70).

The LEED experiment on the stable {110} surface revealed patterns with sharp diffraction spots and low background. Intensity data were collected with the television-camera-microcomputer system described elsewhere⁴ in the energy range 30–210 eV. The data were normalized and corrected for contact-potential difference and background. Two data sets were used in the analysis described below: one at normal incidence ($\theta = 0^\circ$), including 24 (10 nondegenerate) LEED spectra, the other at $\theta = 15^\circ$, $\theta = 90^\circ$, including 18 (12 nondegenerate) spectra. Indexing of the spectra was done according to the convention that, in direct space, assigns the x direction to the shorter interatomic distance (i.e., along $\langle 110 \rangle$) on a {110} plane.

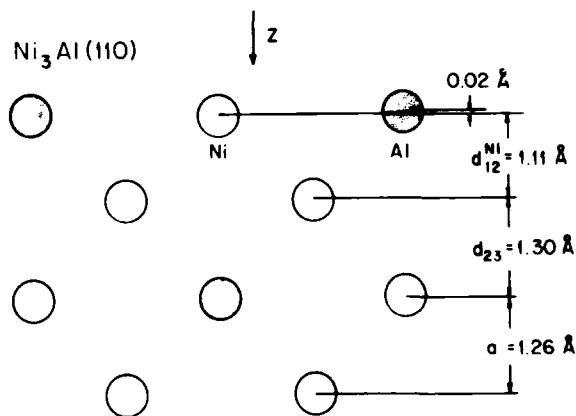


FIG. 6. Schematic side view of the structure of Ni_3Al {110}.

III. ANALYSIS

The intensity calculations were done with the CHANGE program⁵ [6 phase shifts, 79 beams, initial value of inner potential $V_0 = -(10 + 3.5i)$]. The first stage of the analysis was limited to the normal-incidence set. Calculations made for both types of possible terminations showed (both by visual and r -factor⁶ comparisons with experiment) that the mixed layer is first and the all-Ni layer second. In the refinement, the relaxation was investigated by making calculations for several values of the first interlayer spacing d_{12} (bulk value 1.259 Å): expansions and contractions up to 0.15 Å in steps of 0.05 Å were considered. Best fit to experiment was achieved for a contraction of 0.13 Å. Next, buckling of the top layer was tested by allowing the Ni subplane to be 0.05 or 0.1 Å below or above the Al subplane, and simultaneously varying the spacing between the (buckled) first and the (planar) second layer. Under these conditions, the global minimum in r factor was found for $\Delta d_{12} = -0.135$ Å (where d_{12} is the distance between the Al subplane in the first layer and the second layer), and a very slight separation between Al and Ni subplanes in the first layer (Ni being closer to the second layer by 0.015 Å, i.e., the contraction of the Ni subplane is 0.15 Å).

Having found a relatively large relaxation of the first interlayer spacing (10.7% contraction with respect to the bulk value) we considered it advisable to investigate the possible relaxation of the second interlayer spacing d_{23} . Keeping the buckled first layer rigid, and varying independently d_{12} (as defined above) and d_{23} , we found best agreement with experiment for $\Delta d_{12} = -0.135$ Å (as above) and $\Delta d_{23} = +0.039$ Å (or 3.1% of bulk value).

With these parameters we extended the analysis to the non-normal-incidence data. Although the measured angles of incidence for these data were $\theta = 15^\circ$ and $\phi = 90^\circ$ (for the definitions of θ and ϕ see, e.g., Ref. 7), we made calculations for $\theta = 13^\circ$ and $\theta = 17^\circ$ as well. The minimum r factor was found for the set at the measured values of the angles of incidence.

We present the final results of the analysis in Tables I and II for the sets at $\theta = 0^\circ$ and at $\theta = 15^\circ$, $\phi = 90^\circ$, respectively. For the former, the mean r factor is 0.14 for a total energy range ΔE of 2958 eV and a value of 13 eV for the real part of the inner potential V_0 ; for the latter, $\bar{r} = 0.13$ for $\Delta E = 2189$ and $V_0 = 12$ eV. A visual evaluation of the fit of theory to experiment is offered by Figs. 3, 4, and 5. Figure 3 depicts examples of very good fit, Fig. 4, examples of good to mediocre fit, and Fig. 5, examples of poor fit.

IV. CONCLUSIONS

Figure 6 summarizes the final model for the structure of $\text{Ni}_3\text{Al}\{110\}$ in the form of a schematic side view. The top layer has 50% Ni and 50% Al composition, the two subplanes being separated by 0.015 ± 0.03 Å (1.2% of the bulk interlayer spacing 1.259 Å) with the Al subplane farther away from the second layer. The contraction of the distance between the Ni subplane and the second layer is 0.15 ± 0.03 Å (or 12% of the bulk value, while the corresponding value for the Al subplane is 10.7%). The second layer has 100% Ni composition and its distance from the third atomic layer is expanded by 0.04 ± 0.03 Å (or about 3% of the bulk value). Buckling of the second layer and deeper relaxations have not been tested. The mean relaxations found here are comparable to those found in pure $\text{Al}\{110\}$ of -8.6% or -8.5% for the first and 5.0% or 5.5% for the second interlayer spacing,^{8,9} and are substantially greater than those for the closer-packed $\{001\}$ and $\{111\}$ surfaces. However, the buckling is small, unlike the case of $\text{NiAl}\{110\}$, where the buckling is an 11% effect.

ACKNOWLEDGMENTS

Two of the authors (D.S. and F.J.) are grateful to the Office of Naval Research for partial support of this work. The ingot from which the Ni_3Al sample was obtained was grown by D. Pearson (United Technology Research Center), to whom the authors express their thanks.

*Present address: National Synchrotron Light Source (NSLS), Brookhaven National Laboratory, Upton, NY 11973-5000.

¹D. Sondericker, F. Jona, and P. M. Marcus, paper I, Phys. Rev. B 33, 900 (1986); paper II, Phys. Rev. B 34, 6770 (1986), preceding article.

²See, e.g., D. L. Adams and C. S. Sorensen, Surf. Sci. 166, 494 (1986).

³H. L. Davis and J. R. Noonan, Phys. Rev. Lett. 54, 566 (1985).

⁴F. Jona, J. A. Strozier, Jr., and P. M. Marcus, in *The Structure of Surfaces*, edited by M. A. Van Hove and S. Y. Tong

(Springer, Berlin, 1985), p. 92.

⁵D. W. Jepsen, H. D. Shih, F. Jona, and P. M. Marcus, Phys. Rev. B 22, 814 (1980).

⁶E. Zanazzi and F. Jona, Surf. Sci. 62, 61 (1977).

⁷F. Jona, J. Phys. C 11, 4271 (1978).

⁸J. N. Anderson, H. B. Nielsen, L. Petersen, and D. L. Adams, J. Phys. C 17, 173 (1984).

⁹J. R. Noonan, H. L. Davis, and W. R. Erley, Surf. Sci. 152, 142 (1985).



| | |
|--------------------|-------------------------------------|
| Accession For | |
| NTIS GRA&I | <input checked="" type="checkbox"/> |
| DTIC TAB | <input type="checkbox"/> |
| Unannounced | <input type="checkbox"/> |
| Justification | |
| By | |
| Distribution/ | |
| Availability Codes | |
| Dist | Avail and/or Special |
| A-1 | 21 |